Laser Oscillation Diameter Variation Effect on Laser Wire Additive Manufacturing Deposition Morphology

The impacts on weld pool fluctuation, deposited layer morphology, and energy distribution in circular oscillation mode were investigated

BY C. YAN, H. HAN, X. YANG, R. WANG, AND P. ZHANG

Abstract

A high-speed camera was employed to capture the melting process and investigate the impact of laser beam oscillation diameter on weld pool fluctuation and deposition morphology during laser wire additive manufacturing (LWAM) of 316L wire. The transient fluctuations of the weld pool caused by the laser beam were observed at different oscillation diameters. Additionally, 3D morphology measurements were conducted on the deposited layer to assess the effects of different oscillation diameters on its morphology. Further analysis examined the heat dispersion resulting from beam oscillation by plotting the energy distribution for various oscillation diameters. The key findings are as follows: Changes in oscillation diameter resulted in fluctuations within the weld pool that impacted the surface morphology of the deposit and refinement of pore condition as well as alterations in the energy distribution of the weld pool that influenced its contour geometry. Increasing the laser oscillation diameter can effectively make the keyhole shallower, weaken the bottom protrusion of the weld pool, and reduce the curvature of the top surface of the bead. Simultaneously, it can promote the stirring of the liquid solution, effectively refining the porosity area, reducing porosity within the weld pool, and improving the specimen's density. However, larger oscillation diameters lead to more-significant hump arch formation on the deposited surface and larger roughness values.

https://doi.org/10.29391/2025.104.004

Keywords

- Laser Wire Additive Manufacturing
- Oscillation Diameter
- 3D Morphology
- Energy Distribution

Introduction

In recent years, laser wire additive manufacturing (LWAM) has gained widespread use in industrial applications, including surface treatment and additive manufacturing. This is attributed to its benefits such as high efficiency of deposition, rapid cooling rate, favorable refined microstructures, minimal heat input distortion, environmentally friendly production process, and significant manufacturing flexibility (Ref. 1). The Gaussian beam is the current energy source of laser additive manufacturing. Its energy distribution is very concentrated and interacts with the high thermal gradient of the weld pool. Instability and other factors will lead to unsatisfactory deposition quality of additive parts during processing, resulting in defects such as cracks and pores (Ref. 2). Several scholars have studied controlling weld pool defects in laser additive manufacturing. A recent oscillation strategy that alters the laser energy distribution of the beam to suppress porosity and splatter defects has garnered significant attention. This approach holds promise as one of the future directions of laser additive technology (Refs. 3–7).

Beam oscillation gained attention due to its favorable performance in welding applications. As a result, numerous scholars have conducted extensive research on beam oscillation strategy in laser additive manufacturing and laser welding. In this regard, Wu et al. (Ref. 8) showed that the spreading of liquid metal in narrow gap grooves increased gradually when the oscillation diameter and frequency were increased. The laser spot's rapid localized movement improved the keyhole's stability, accelerated the weld pool's flow rate, and reduced the solidification time. Jiang et al. (Ref. 9) conducted a study to investigate the impact of oscillating geometry on vacuum laser beam welding by utilizing defocusing conditions to oscillate weld thick-sectioned aluminum alloys. The research revealed that linear oscillating welds displayed more severe porosity defects, while figure-eight oscillations facilitated better welding formation due to higher laser travel speeds and enhanced stirring capabilities. Chen et al. (Ref. 10) proposed the concepts of average linear energy density (E) and average travel speed (v) during the laser welding process. They observed that sinusoidal oscillation welding can homogenize energy distribution, reduce energy peaks, and play a key role in limiting weld fusion depth.

Wu et al. (Ref. 11) utilized synchrotron-based x-ray in-situ techniques to observe dynamic keyhole oscillations during the fusion of Ti-6Al-4V micro-powder beds. The oscillating beam decreased the aspect ratio of the weld pool by using the same laser power and speed in the experiment. Lei et al. (Ref. 12) investigated using a circular oscillating laser for preparing ceramic WC/NiCu composites. They found that the circular oscillating laser mode, operating at a specific frequency, resulted in a more uniform distribution of temperature gradients in the weld pool. Bernauer at al. (Ref. 13) conducted experiments involving different processes of 316L laser-fused wires by adjusting the focal position of the laser beam to create an annular laser spot with a 2.75 mm outer diameter. At elevated weld pool temperatures, the volume of the deposited weld channel increased significantly in proportion to the weld pool's volume. Liu et al. (Ref. 14), by utilizing a circular oscillating laser mode and wire feeder from both sides of the laser head, achieved bilinear additive manufacturing. The study demonstrated that the oscillation frequency was inversely related to the weld pool's width, with a higher frequency improving forming quality.

Despite extensive research on welding and additive manufacturing processes involving beam oscillation strategies by numerous scholars, there remains a deficiency in process monitoring and morphology control for ensuring the stability of laser wire additive manufacturing. This study utilized high-speed cameras to observe the laser additive material process with varying oscillation diameters. It investigated the impact of different laser oscillation diameters on weld pool fluctuation, deposited layer morphology, and energy distribution in the circular oscillation mode.

Fig. 1 — Laser additive manufacturing system.

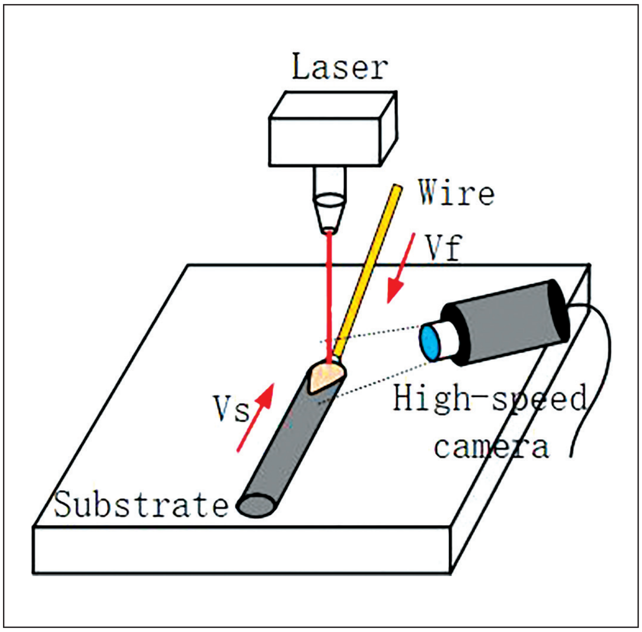

Fig. 2 — Schematic diagram of high-speed camera shooting.

Materials and Methods

The LWAM experiment utilized the HY-PTBZGQ-1000 fiber laser additive manufacturing system, as illustrated in Fig. 1. This system comprises the MFSC-1000X fiber laser, the DI-2000L oscillation laser head, the QL-1000 wire feeder, the CNC coordinate table, and the control system. The fiber laser has a maximum power of 1000 W and operates at a wavelength of 1080 nm, and the focal length of the laser head is 200mm. The Galvo scanning system inside the laser head can be programmed to oscillate the beam in a desired pattern. The minimum waist of the beam was located at the surface of the substrate, and the minimum spot diameter was 0.15 mm. In this experiment, 0.8mm diameter 316L stainless steel wire was chosen for LWAM on a 50 mm*50 mm*8 mm 316 stainless steel substrate. Refer to Table 1 for the material composition details:

The experiment utilized the circular oscillation mode to perform single-factor oscillation on various diameters in LWAM experiments. The oscillation diameter range A was set from 0 to 1.4 mm with intervals of 0.2 mm, divided into eight experimental groups. Before experimenting, the oxidized layer of the deposited substrate was removed using a grinder and cleaned with alcohol. The wire feeder was positioned in front of the laser, and the wire feeding angle was 60 deg. The spacing between the laser and the welding wire was set at 0.2 mm on the substrate plane, with a laser power, P, of 400 W, wire feeding speed, Vf, of 9 mm/s, and scanning speed, Vs, of 4 mm/s. The minimum waist of the beam was located at the substrate's surface, with an Ar gas flow rate of 15 L/min for protective gas. The laser oscillation frequency was set to 46 Hz based on the maximum oscillation frequency of the laser. To ensure the accuracy of the experiment, each group

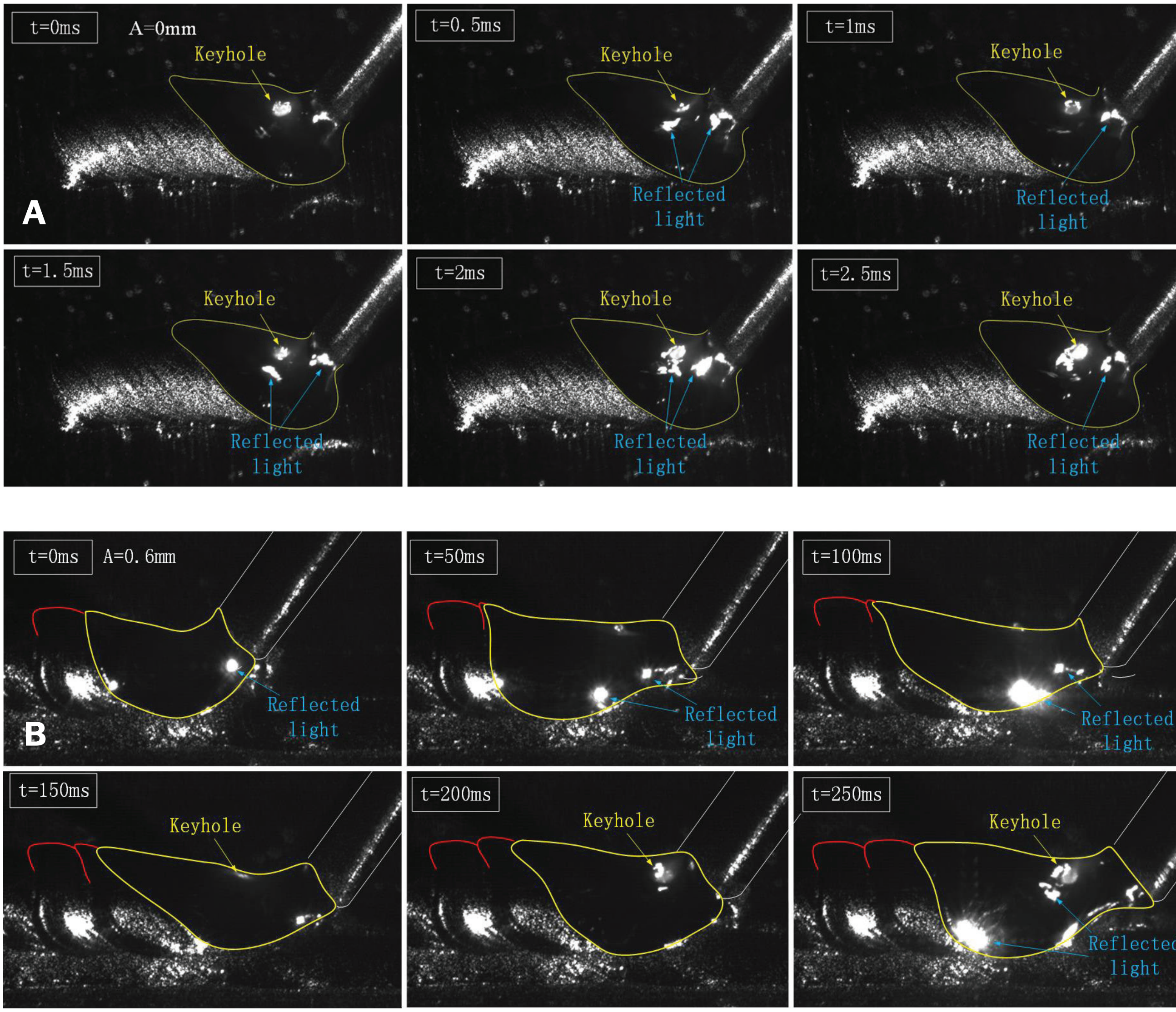

Fig. 3 — Weld pool fluctuation with different oscillation diameters: A — Oscillation diameter A = 0 mm; B — oscillation diameter A = 0.6 mm.

Table 1 — Material Composition of Welding Wire and Substrate (%)

	C	Si	Mn	S	P	Cr	Ni	Mo	N	Cu
316L Wire	0.022	0.42	1.89	0.007	0.009	19.12	12.62	2.62	0	0.34
316 Substrate	0.043	0.46	1.12	0.003	0.027	18.15	10.01	2.1	0.031	0

of experiments was repeated five times. Table 2 presents the experimental parameters of the LWAM process.

The additive manufacturing process was captured using a high-speed Techtronics camera, as depicted in Fig. 2. The camera system includes the AcutEye high-speed image system V4.0 for data acquisition during the fusing process, featuring a 100 W power 910 nm wavelength parallel auxiliary laser light source and a 910 nm wavelength narrow band filter for precise light filtering observations. Operating at a frame rate of up to 4000 Hz, the camera can adjust the irradiation range and light intensity of the auxiliary laser light source. The camera lens utilized a variable focal length lens with a minimum objective distance of 12 mm. Positioned correctly

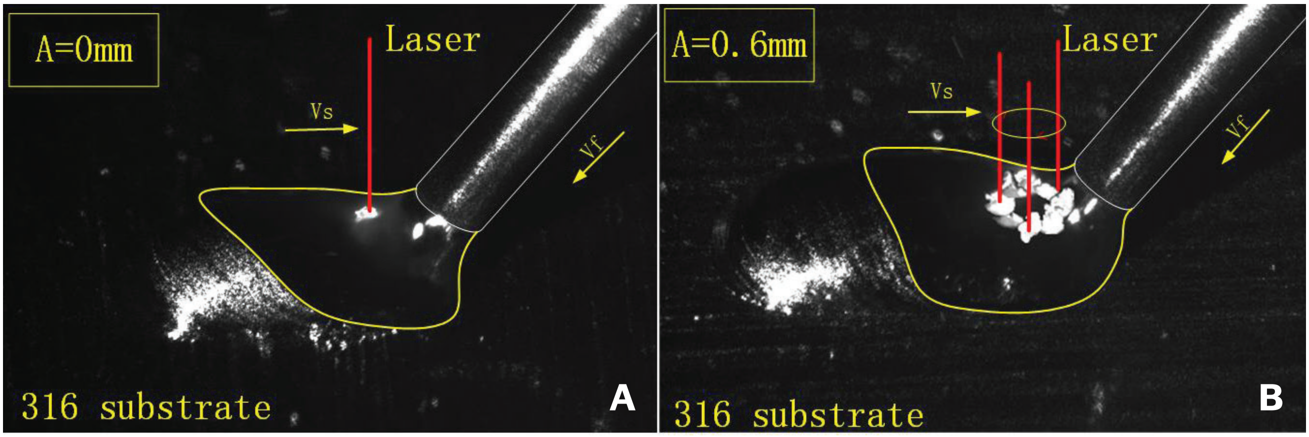

Fig. 4 — Variation of scanning path of beam spot with different oscillation diameters: A — Oscillation diameter A = 0 mm; B — oscillation diameter A = 0.6 mm.

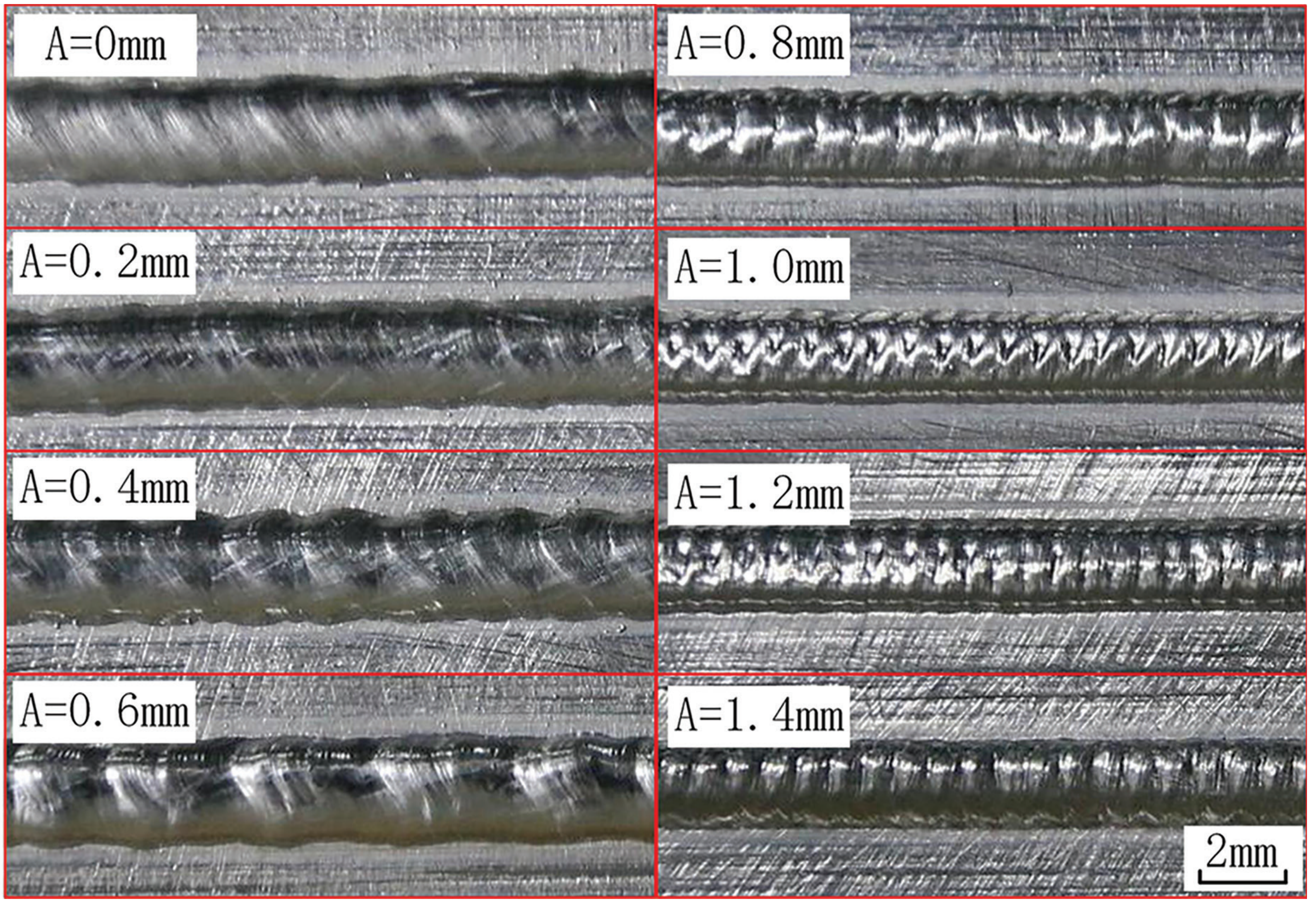

Fig. 5 — Surface morphology of the LWAM deposit.

in the deposition direction, both the camera and auxiliary light source were set at a top-down shooting angle of 70 deg relative to the substrate, and the angle between camera axis and travel direction was 90 deg.

Firstly, the LWAM sample was treated with stainless steel pickling and passivation paste to eliminate surface oxidation coatings. Subsequently, the topography of the bead surface was documented using a Canon 70D DSLR camera, while a KEYENCE LJ-X8000A laser topography meter performed three-dimensional topography scanning under different laser oscillation modes. Following this, specimens deposited in different oscillation modes were initially line-cut along the hump position, and the cutting surfaces were subjected to metallographic mosaic. The specimens were then ground, polished, and etched in 316L special corrosion solution to observe the weld pool. The etchant had a ratio of hydrofluoric acid: hydro-

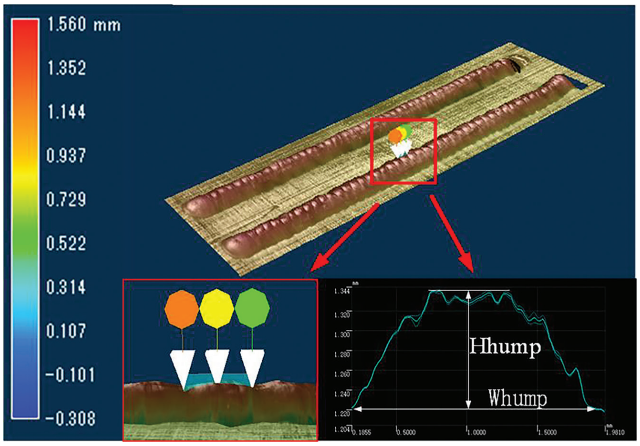

Fig. 6 — 3D morphology of the hump.

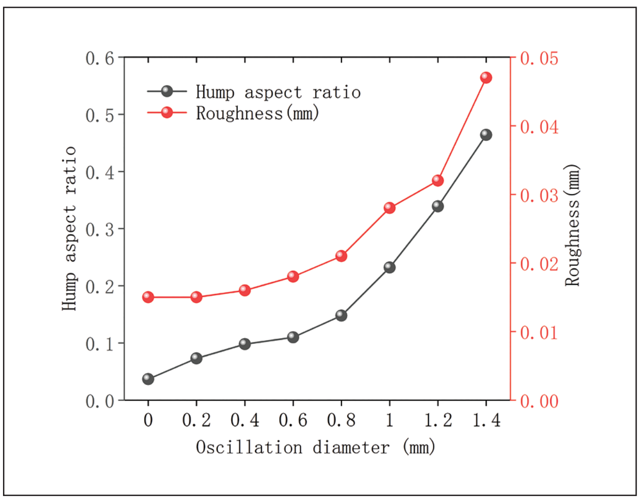

Fig. 7 — Variation of hump aspect ratio and roughness of the hump.

chloric acid: nitric acid: water = 1:2:3:4, which allowed for clear observation of the weld pool. Furthermore, metallographic observation of the deposited specimen sections was carried out using an optical microscope, and data extraction from the images was conducted using Image J software.

Results

Fluctuations in the Weld Pool

The laser melting process was observed by selecting photographs at different time points to analyze the weld pool's fluctuation. Fig. 3 illustrates the weld pools corresponding to different oscillation diameters.

In Fig. 3, the laser beam was irradiated on the substrate to create a weld pool, and a liquid-bridge transition mode persisted between the leading edge of the weld pool and the feeding wire. The continual melting and fusion actions of the wire dictated the flow direction of the weld pool, and due to the interaction between the introduction of the welding wire at the front and solidification at the back, a distinct clockwise vortex was formed at the back bottom of the weld pool. In Fig. 3A, the keyhole of the weld pool progressed linearly with the laser head in the absence of oscillation, and it remained situated above the weld pool with periodic closed openings. Weld pool fluctuation was not apparent, and the resultant deposition layer at the back of the weld pool exhibited uniform morphology and a glossy surface finish.

However, after oscillation was introduced, the liquid weld pool exhibited fluctuation. The keyhole of the weld pool rotated clockwise around the laser head's central axis, forming an irregular fish-scale pattern of varying heights. As the oscillation diameter increased, the intensity of weld pool fluctuation also amplified, particularly when the oscillation diameter reached 0.6 mm. In Fig. 3B, the weld pool's size gradually elongated during the time interval t = 0–100 ms, followed by a subsequent reduction in size during t = 100–200 ms. This periodic expansion and contraction of the weld pool resulted in its transformation from a flat fish-scale pattern to a periodic hump morphology as the cooling process ensued. Notably, the formation time of a single hump was approximately 200 ms, which did not align with the oscillation frequency of the laser.

Positional Changes of the Spot in Weld Pool

To visualize the beam spot paths of the weld pool under different oscillation diameters, we assembled 15 continuous photographs to depict the spot paths accurately. The resulting scanning paths are shown in Fig. 4 for the oscillation diameters of 0 and 0.6 mm.

In Fig. 4, a keyhole emerged on the surface of the weld pool due to the intense laser energy beam and the recoil force of the weld pool. Notably, variations in the keyhole's positional changes were observed when the weld pool spot was irradiated with laser oscillations of different diameters. Specifically, with an oscillation diameter of 0 mm, the laser spot within the keyhole progressed horizontally in alignment with laser head movement. After introducing an oscillation diameter, the laser beam generated a large circular annular spot above the weld pool.

Surface Morphology of Deposited Specimens

The surface morphology of the LWAM deposits with varying oscillation diameters and the 3D morphology of the hump on the deposited specimen's surface are illustrated in Figs. 5 and 6, respectively.

Fig. 5 demonstrates the notable variation in the topography of the bead surface as the oscillation diameter changed. Specifically, the uniformity of the bead surface was optimized when the laser beam oscillated at a diameter of 0. However, for oscillation diameters larger than 0.4 mm, hump formation occurred on the bead surface, with a relatively uniform distribution across the bead surface. The hump height, hump width, and top roughness along the deposition direction were measured, and the measurement process was repeated five times for each specimen group to obtain the average value.

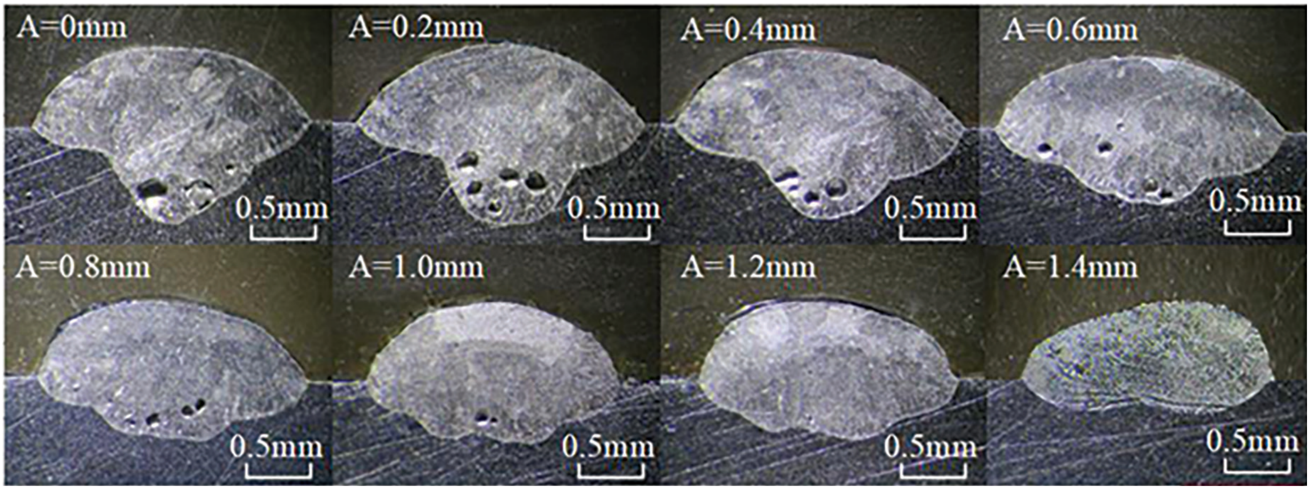

Fig. 8 — Cross-section of the weld pool with different oscillation diameters.

Table 2 — Experimental Parameters of LWAM

P (w)	Vf (mm/s)	Vs (mm/s)	D (mm)	A (mm)
400	4	9	0	0–1.4

Fig. 7 illustrates the changes in the hump and roughness with varying oscillation diameters.

The hump width gradually diminished as the oscillation diameter rose while the hump height continued to increase. The overall hump geometry evolved from initially flat, short protrusions to progressively steeper protrusions. The hump aspect ratio (Hhump/Whump) and roughness values all increased with the increase of the laser spot's oscillation diameter.

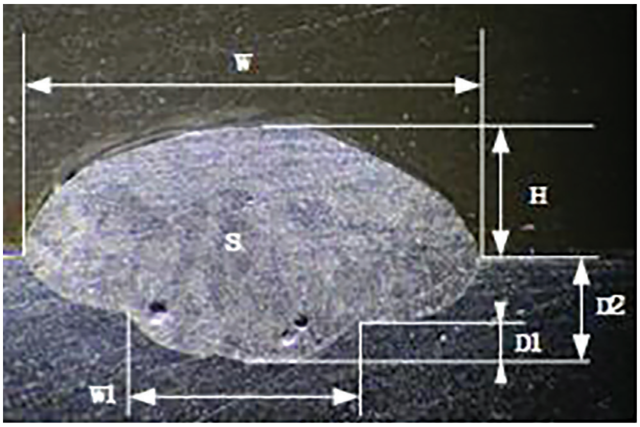

Fig. 9 — Measurement of the weld pool cross-section.

Cross-Sectional Geometry of Deposited Specimens

The cross-section geometries of the LWAM weld pool zones with varying oscillation diameters are depicted in Fig. 8.

As depicted in Fig. 8, the oscillation diameter substantially influenced the deposited layer's cross-sectional profile geometry. By observing the top profile of the weld pool, it is evident that increasing the oscillation diameter significantly reduced the curvature of the top surface of the bead. Additionally, the bottom profile of the weld pool was examined, and it was observed that there was a distinct step protrusion at the bottom when the laser oscillation diameter was below 1.0 mm. When the oscillation diameter was 0 mm, the bottom profile of the weld pool formed a sharp protrusion. As the oscillation diameter increased, the bottom of the weld pool transitioned from a sharp protrusion to a bowl-shaped protrusion. Notably, when the oscillation diameter reached 1.4 mm, the laser oscillation diameter effectively reduced the depth of the keyhole in the weld pool. It diminished the protrusion at the bottom of the weld pool.

The dimensions of the weld pool's cross-section for various oscillation diameters were extracted from the metallographic images using Image J software. Measurements of the weld pool's cross-section dimensions are shown in Fig. 9.

The weld pool width (W), weld pool height (H), weld pool depth (D2), weld pool area (S), dilution rate (η), wetting angle, protrusion width (W1), protrusion depth (D1), average pore area (P1) and total pore volume (P) of the weld pool for different oscillation depositions are illustrated in Fig. 10.

The variation in oscillation diameter exerted a significant influence on the cross-section geometry of the weld pool. As depicted in Fig. 10A, the weld pool's width remained constant when the oscillation diameter was below 0.4 mm, peaked at 0.6 mm, and then decreased as the oscillation diameter continued to increase. The width of the bottom protrusion of the weld pool remained relatively stable. The alteration in the bottom protrusion's depth aligned with the weld pool's depth change exhibited a decreasing trend with increasing oscillation diameter. This observation confirmed that increasing the laser oscillation diameter can notably reduce the weld pool's depth and effectively diminish the protrusion at the bottom of the weld pool. The weld pool's height showed minimal variation with the increasing oscillation diameter. As depicted in Fig. 10B, the weld pool's area

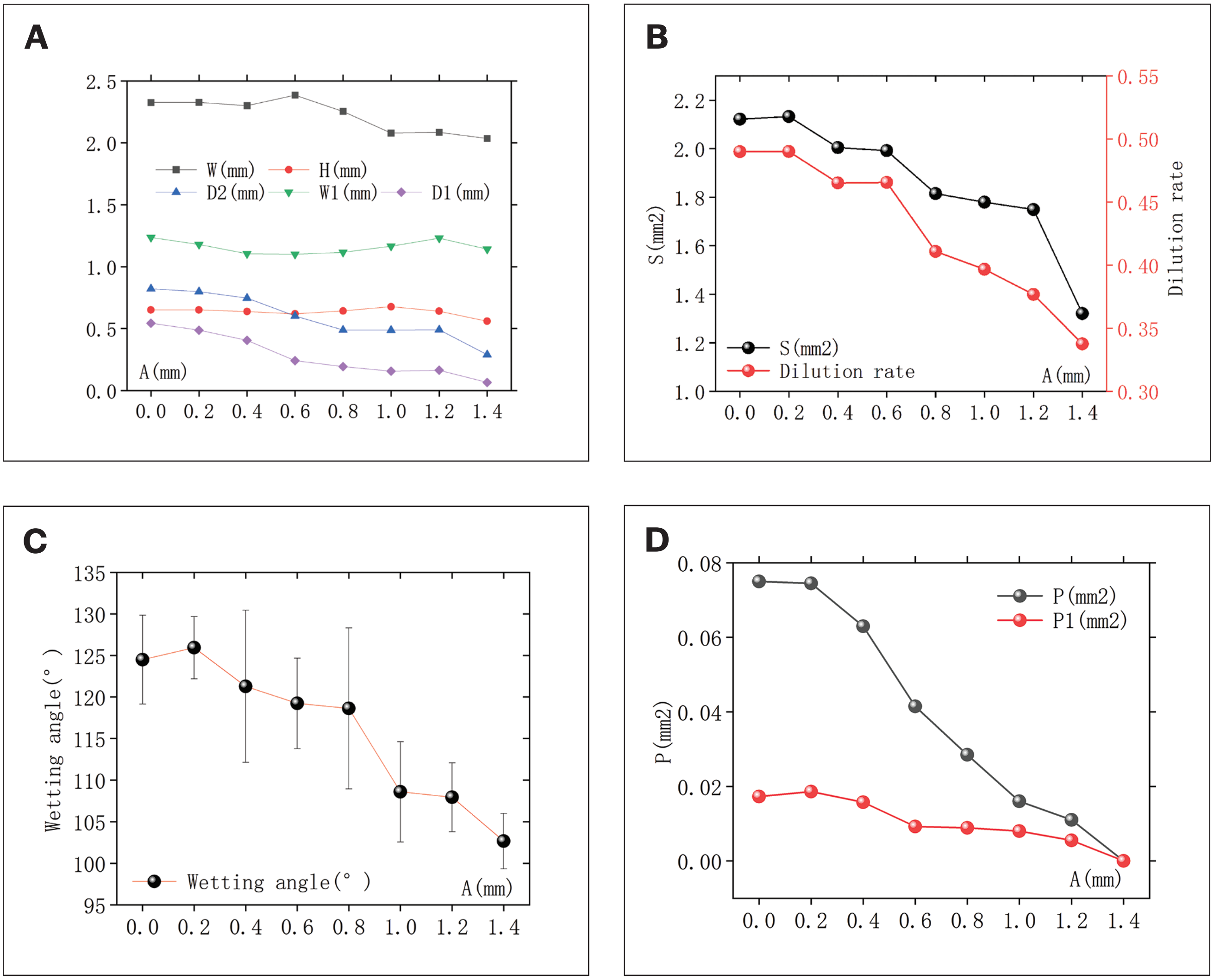

Fig. 10 — Dimensions of weld pool geometry with different oscillation diameters: A — Variation of weld pool size and protrusion size; B — variation of weld pool area and dilution rate; C — variation of wetting angle; D — variation of porosity conditions.

and dilution rate decreased with the increasing oscillation diameter. As illustrated in Fig. 10C, the wetting angle of both sides of the weld pool gradually decreased as the oscillation diameter increased. As depicted in Fig. 10D, the porosity variation inside the weld pool became notably evident with increasing oscillation diameter, primarily concentrated in the step-shaped protruding areas. Initially, when the oscillation diameter was 0 mm, large pores were present inside the weld pool because of the poor choice of focus condition, and their area gradually decreased as the oscillation diameter increased. At 0.6 mm oscillation diameter, relatively small pores replaced the large ones, and at 1.4 mm oscillation diameter, no pores were observed inside the weld pool. The average area of individual pores within the weld pool decreased as the oscillation diameter increased, indicating that the regular oscillation of the laser beam induced liquid agitation. Moreover, increasing the oscillation diameter effectively refined the pore area, reducing the weld pool's internal porosity and enhancing the deposit's densification.

Discussion

To elucidate the impact of laser oscillation on the change in weld pool profile, it is essential to analyze the distribution of laser heat input in various oscillation modes (Ref. 15). In the LWAM process, the laser head undergoes horizontal movement along the deposition direction. At the same time, the beam is scanned in a circular shape around the central axis of the laser head. The combination of the laser head's horizontal movement and the beam's rotary oscillation motion form the helical trajectory path of the beam. The scanning trajectory of the light spot under different oscillation diameters is depicted in Fig. 11.

In Fig. 11, it is evident that the laser oscillation trajectory was more concentrated with a small oscillation diameter. As the laser oscillation diameter increased, the time-averaged area of the laser spot irradiated on the substrate plane also increased. The variation of the laser oscillation trajectory directly affected the effective power density of the laser irradiation on the substrate. By integrating the effective laser power density along the deposition direction during an oscillation period, it was possible to obtain the laser energy input at different positions in the weld pool-width direction. The equations for calculating the laser energy input E for different oscillation diameters are provided below:

$$E = \int_{0}^{L_1} P_{D1} \tag{1}$$

$$PD_1 = PD/L \tag{2}$$

$$PD = P/(\pi * \omega^2) \tag{3}$$

In the given equation, PD_1 represents the effective power density in various oscillation modes, while *PD* signifies the power density of the laser spot. The length of the rotating spot trajectory varies across different oscillation modes and is denoted by *L*, *P* corresponds to the laser output power of 400 W and ω represents the minimum laser spot size radius of 0.095 mm in the focused state. The effective power density and energy input in the direction of the weld pool for different oscillation diameters of the laser were calculated by the above equations, and the laser energy input, *E*, and energy distribution at different oscillation diameters are shown in Figs. 12 and 13.

As shown in Fig. 12, the laser energy input showed a decreasing trend with increasing oscillation diameter. As shown in Fig. 13, when the oscillation diameter was 0 mm, the laser energy input was the most concentrated. As the oscillation diameter increased, the laser energy input gradually leveled off from the initial high concentration. Considering the protrusion at the bottom of the weld pool and the porosity within the weld pool, as illustrated in Fig. 8, it can be inferred that the weld pool's bottom morphology was influenced by the laser energy distribution resulting from oscillation motion. An increase in the oscillation diameter can effectively reduce the effective energy density, leading to a more uniform distribution of laser energy input on both sides of the deposited layer. When the oscillation diameter was 0 mm, the laser's effective power density was most concentrated, facilitating the formation of a sharp downward angle protrusion and a significant depth of melting in the weld pool. This decreased fusion depth reduced the likelihood of porosity overflowing the keyhole closure, thereby minimizing the formation of large porosity defects. With an increase in oscillation diameter, the effective power density of the weld pool gradually decreased, and the heat flow density decreased significantly. As a result, the keyhole depth effectively improved, and the pores were more likely to overflow to the outside, forming dense deposits without internal pores. The dispersion of laser heat source energy also weakened the protrusion at the bottom of the weld pool, resulting in a flatter bottom for the deposited layer.

When considering the energy distribution of the weld pool and the hump formation on the surface of LWAM-deposited specimens, as shown in Fig. 5, it can be observed that an increase in oscillation diameter dispersed the heat source energy outward. The surface tension of the liquid decreased

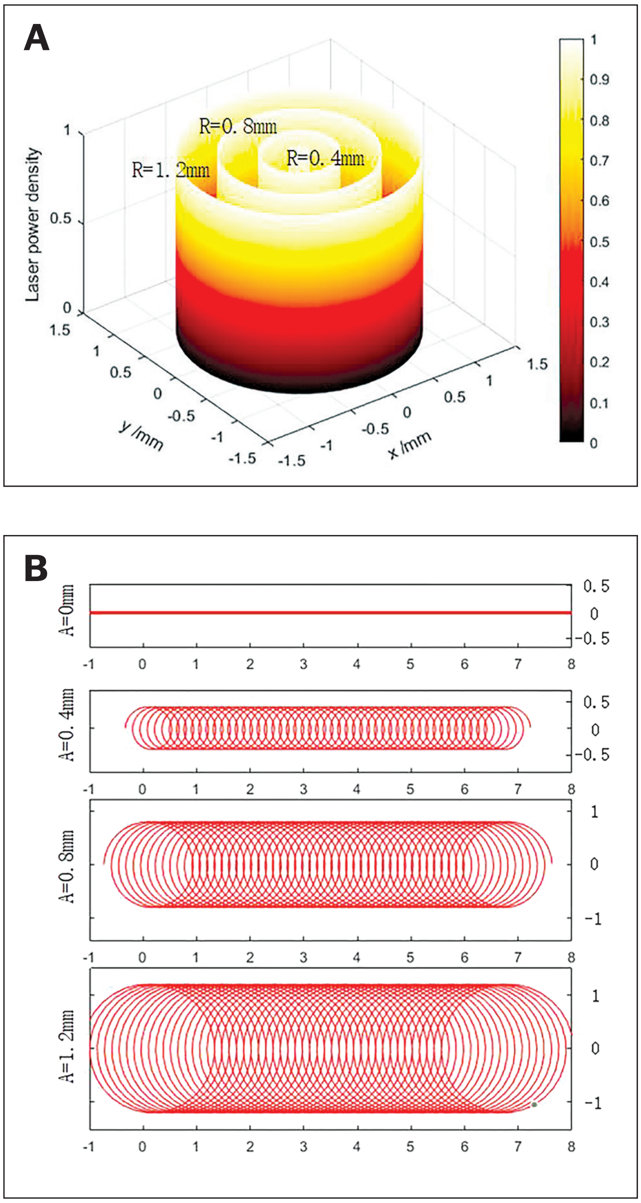

Fig. 11 — Scanning trajectory of laser spot with different oscillation diameters: A — Rotation of laser with different oscillation diameters; B — spiral trajectory lines of light spots with different oscillation diameters.

with increasing temperature. In the beam oscillation mode, the energy was dispersed outward due to the increase in the irradiation volume, thus reducing the temperature of the weld pool. This dispersion caused the surface tension of the liquid weld pool to increase, made it more prone to shrinkage, and formed a shorter weld pool at t = 0 ms, as shown in Fig. 3B. As the laser heat source continued to input heat, the energy of the weld pool accumulated. At t = 100 ms, as depicted in Fig. 3B, the weld pool's surface tension decreased, resulting in its spreading and elongation. Due to the interplay between wire feed rate and melting, heat absorption, substrate heat transfer, and spot rotational oscillation, the weld pool underwent periodic fluctuations. The hump formation occurred

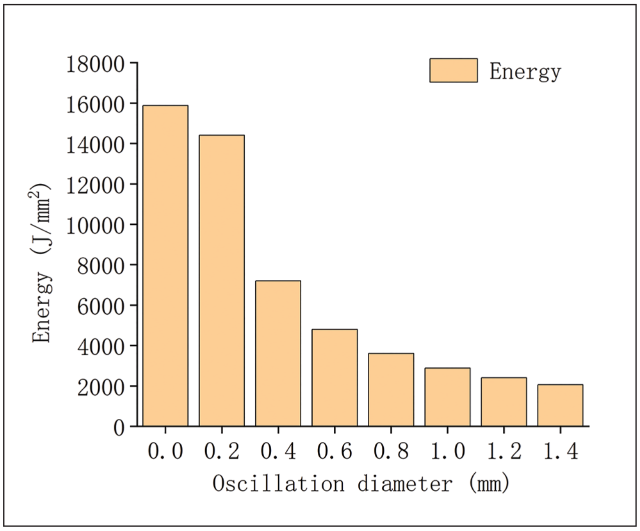

Fig. 12 — Heat source energy for different oscillation diameters.

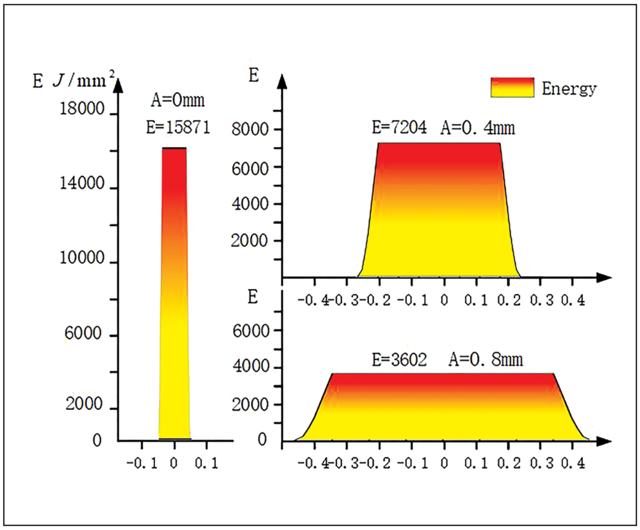

Fig. 13 — Schematic of energy distribution.

as a result of these periodic fluctuations driven by the contraction of surface tension. The higher surface tension of the weld pool led to more-pronounced arching, which, in turn, decreased the roughness of the cooled deposited layer with increasing oscillation diameter.

When considering the increase of hump aspect ratio and roughness, values changed with the increase of the laser spot's oscillation diameter in Fig. 7. This phenomenon demonstrated that the weld pool underwent periodic fluctuations due to beam rotation, rapid heat transfer, and substrate cooling, leading to the formation of protruding hump structures. A higher temperature difference resulted in steeper protrusions and deteriorated the surface roughness of the deposited material.

Considering the cross-section geometry of the LWAM weld pool with varying oscillation diameters in Fig. 8 suggests that for relatively small oscillation diameters, the depth of the keyhole is much deeper than the depth of the heat-conducting weld pool formed by the laser beam's heat conduction.

When considering the weld pool's area and dilution rate with the increasing oscillation diameter, as depicted in Fig. 10B, this observation suggests that the increased oscillation diameter reduced the keyhole depth of the weld pool, leading to a weakened inverse bremsstrahlung absorption in the inner wall of the weld pool's keyhole. Consequently, the reduced keyhole depth diminished the energy absorption inside the weld pool, resulting in a decrease in both the volume of the weld pool and the dilution rate. When considering the wetting angle changes, as illustrated in Fig. 10C, and the change in curvature of the contour line at the top of the weld pool, it can be analyzed that the increased oscillation diameter enhanced the internal energy distribution within the weld pool, causing more heat to be dispersed toward the sides. This effectively reduced the surface tension of the liquid weld pool during the melting process and improved the surface morphology of the deposit.

The analysis above indicates that the weld pool's width, depth, full weld pool area, and dilution rate all decrease with increasing oscillation diameter. This demonstrates that increasing the oscillation diameter of the laser spot weakens the formation of a keyhole at the weld pool's depth, reduces keyhole energy absorption, disperses heat at the weld pool's edge, increases the surface temperature of the weld pool, and enhances the boundary wetting effect. As a result, a relatively smooth surface profile of the deposition layer is formed, leading to a high-quality deposition layer without pores.

Conclusions

1. Variations in oscillation diameter result in fluctuations in the weld pool and affect the accuracy of the bead surface. As the oscillation diameter increased, the intensity of weld pool fluctuation gradually increased. Additionally, the morphology of the final deposition surface changed from a flat and uniform fish-scale pattern to a periodic protruding hump structure. Increasing the diameter of the oscillation led to more-pronounced arching of the humps on the bead surface and, consequently, higher roughness values.

2. Variations in oscillation diameter influence the geometry of the weld pool's profile. As the oscillation diameter increased, the bottom of the weld pool transitioned from an initial sharp protrusion to a bowl-shaped protrusion and eventually evolved into a horizontal step-like protrusion. Increasing the laser oscillation can effectively decrease the depth of the keyhole in the weld pool, reduce the protrusion at the bottom of the weld pool, and enhance the curvature of the deposit's apex.

3. Variations in oscillation diameter can effectively limit the volume fraction of the weld pool's porosity. As the oscillation diameter increased, the total pore volume and the average pore size of the weld pool gradually decreased, and the densification of the deposited layer was enhanced.

4. The addition of oscillation can increase the spot trajectory path, reduce the effective power density, homogenize the energy distribution of the weld pool, and improve the boundary wetting effect to form a smoother deposition profile with a smaller wetting angle.

Declaration of conflicting interests

The author(s) declared no potential conflicts of interest with respect to the research, authorship, and/or publication of this article.

Funding

The author(s) disclosed receipt of the following financial support for the research, authorship, and/or publication of this article: This work was supported by the National Natural Science Foundation of China (51375146); Ministry of Industry and Information Technology of the People's Republic of China (2018ZNZX01-02) and Natural Science Foundation of Henan Province (17A460012).

References

1. Abuabiah, M., Mbodj, N. G., Shaqour, B., Herzallah, L., Juaidi, A., Abdallah, R., and Plapper, P. 2023. Advancements in laser wire-feed metal additive manufacturing: A brief review. *Materials* 16(5): 2030. DOI: 10.3390/ma16052030

2. Bi, J., Wu, L., Li, S., Yang, Z., Jia, X., Starostenkov, M. D., and Dong, G. 2023. Beam shaping technology and its application in metal laser additive manufacturing: A review. *Journal of Materials Research and Technology* 26: 4606–4628. DOI: 10.1016/j.jmrt.2023.08.037

3. Pamarthi, V. V., Sudarsan, C., Das, A., Hazra, S., and Panda, S. 2023. Study of beam wobbling technique and porosity formation in laser welding of ultra-thin AA1050 sheet—Microstructural and mechanical analysis. *The International Journal of Advanced Manufacturing Technology* 129: 4011–4029. DOI: 10.1007/s00170-023-12493-9

4. Yoon, H., and Bang, H. 2023. The effect of wobbling on the welding characteristics in Al/Cu fiber laser welded joints. *The International Journal of Advanced Manufacturing Technology* 127: 5343–5352. DOI: 10.1007/s00170-023-11653-1

5. Asirvatham, C., Collins, S., and Masters, I. 2022. Laser wobble welding of steel to aluminium busbar joints for Li-ion battery packs. *Optics & Laser Technology* 151(7): 108000. DOI: 10.1016/j.optlastec.2022.108000

6. Song, D., Kim, R., Choi, K., Shin, D., and Lee, S.-J. 2023. Effects of beam shape on the microstructures and mechanical properties during thin-foil laser welding. *Metals* 13(5): 916. DOI: 10.3390/met13050916

7. Elmer, J. W., Vaja, J., Carpenter, J. S., Coughlin, D. R., Dvornak, M. J., Hochanadel, P. Gurung, P., Johnson, A., and Gibbs, G. 2020. Wire-based additive manufacturing of stainless steel components. *Welding Journal* 99(1): 8-s to 24-s. DOI: 10.29391/2020.99.002

8. Wu, P., Wang, M., Fang, N., Xu, K., Sun, L., Huang, R., and Qin, J. 2023. Analysis on the technology, microstructure, and mechanical properties of Ti-6Al-4 V alloy narrow gap oscillation laser welding with multi-stranded wire. *The International Journal of Advanced Manufacturing Technology* 128: 729–742. DOI: 10.1007/s00170-023-11881-5

9. Jiang, N., Jiang, M., Chen, X., Han, T., Ma, S., Chen, Y., Wang, Z., Jiang, Y., Yang, L., Lei, Z., and Chen, Y. 2023. Effect of beam oscillation on weld formation, microstructure and mechanical properties in vacuum laser beam welding of thick section 5083 aluminum alloy. *Optics & Laser Technology* 171(4): 110408. DOI: 10.1016/j.optlastec.2023.110408

10. Chen, L., Mi, G., Zhang, X., and Wang, C. 2021. Effects of sinusoidal oscillating laser beam on weld formation, melt flow and grain structure during aluminum alloys lap welding. *Journal of Materials Processing Technology* 298(12): 117314. DOI: 10.1016/j.jmatprotec.2021.117314

11. Wu, Z., Tang, G., Clark, S. J., Meshkov, A., Roychowdhury, S., Gould, B., Ostroverkhov, V., Adcock, T., Duclos, S. J., Fezzaa, K., Immer, C., and Rollett, A. 2023. High frequency beam oscillation keyhole dynamics in laser melting revealed by in-situ x-ray imaging. *Communications Materials* 4(1): 5. DOI: 10.1038/s43246-023-00332-z

12. Lei, J., Liu, G., Li. H., Han, H., Di, R., and Lei, J. 2023. Gaussian and circular oscillating laser directed energy deposition of WC/NiCu composites. *Materials Characterization* 204(10): 113218. DOI: 10.1016/j.matchar.2023.113218

13. Bernauer, C., Zapata, A., and Zaeh, M. F. 2022. Toward defect-free components in laser metal deposition with coaxial wire feeding through closed-loop control of the melt pool temperature. *Journal of Laser Applications* 34(4): 042044. DOI: 10.2351/7.0000773

14. Liu, M., and Long, J. 2023. Study on process parameters of aluminium alloy oscillating laser double-wire additive manufacturing. *Journal of Physics: Conference Series* 2499(1): 012004. DOI: 10.1088/1742-6596/2499/1/012004

15. Xia, P., Wang, C., Mi, G., Zhang, M., Xiong, L., Zhang, X., Zhai, C., Feng, F., and Hu, Y. 2023. Numerical simulation of molten pool flow behavior and keyhole evolution behavior in dual-laser beam oscillating bilateral synchronous welding of T-joints. *International Journal of Heat and Mass Transfer* 209(8): 124114. DOI: 10.1016/j.ijheatmasstransfer.2023.124114

CHENXIAO YAN, **HONGBIAO HAN** (*lyhhb7157@163.com*), **RUI WANG,** and **PENG ZHANG** are with the School of Mechatronics Engineering, Henan University of Science and Technology, Luoyang, China. **XIN YANG** is with AVIC Jonhon Optronic Technology Co. Ltd., Luoyang, China.